8th International Conference on DEVELOPMENT AND APPLICATION SYSTEMS
Suceava, Romania, May 25 – 27, 2006

CAD-TECHNOLOGY FOR THE NERVA HYPERSONIC RECOVERABLE BODY

Radu-Dan RUGESCU
"Politehnica" University of Bucharest
Str.Bancila nr.18, RO-060144 Bucuresti
rugescu@yahoo.com

Abstract. *A potentially genuine launch vehicle, developed from a mass of existing, disabled military rocket vehicles for eventual small, below 100 kg LEO satellites are proposed. Some of the specific technological challenges regarding the definition of tasks and reliability-versus-cost solutions are outlined. The main challenge refers to the requirement for an enhanced, high efficiency, liquid propellant rocket motor, reliable and cheap enough to ensure the working capability of the non-orbital, re-entry NERVA vehicle. The program to investigate potentials in manufacturing high-pressure pumps and turbo-pump units are the background of the NERVA program, a Non-orbital Entry Return Vehicle Assessor. Base pressure prediction and experimental confirmation is addressed in predicting the entry dynamics in the Earth atmosphere. Results of previous base pressure measurements on the bottom of a low drag, hyper velocity re-entry body are compared with other data and unexpected dissimilarities are discussed, in connection with a model for the boundary layer in hypersonic motion. A reconverted SA type missile is proposed as a carrier vehicle for the research platform. Clarification of base pressure measurement data is expected to serve for better predicting the flight characteristics of rocket propulsion systems, while producing the so-called thrust-induced drag in the powered phase of the flight. Base pressure fluctuations are presented as an effect of the high instability of the hypersonic boundary layer that have direct impacts on entry stability and on the flight characteristics of rocket propulsion systems. Validity requirements regarding the correct representation of base pressure measurements on the back-bottom of re-entry bodies are proposed in order to enhance experimental data, marked in the past experience by some uncertainties.*
Keywords: *Rocket vehicle, Atmosphere re-entry, Hypersonic flight, Rocket engines*

1. Introduction

Due to the doubtful evolution of the US Space Shuttle program a number of replacing solutions were found regarding space launchers. Although the main focus everywhere is on the category of large payloads, the number of small to medium sized orbital applications is increasing, under the name of small or even nano-satellites. The development of the joint US-Ukraine “Sea Launch” enterprise enters the role of supplying space carriers of reduced size. The same does the innovative “SpaceX” US enterprise, based on proprietary developed liquid propellant transporters with low thrust-to-weight ratio, convenient for some payloads.

The idea is advanced by ADDA (Association Dedicated to Development in Astronautics) to reconvert existing rocket systems in Romania from military applications to space research vehicles. This can only be achieved if the efficiency of the existing rocket system is drastically improved and one direction of research is the improvement of the rocket motor efficiency, or the specific impulse.

The Shuttle main engine (Pratt & Whitney 1972) is developing 210 bar internal pressure in the combustion chamber where liquid oxygen and hydrogen are pumped at 340 bar by a closed circuit turbo-pump assembly. It delivers 4400 m/s of vacuum specific impulse. It is nevertheless considered that the upper limit of efficiency has not yet been attained and even higher combustion pressures are profitable. The most recent evolution in that respect is the IPD or Integrate Plumbing Demonstrator. One of many innovations being tested by the Air Force and NASA is to send all of the fuel and oxidiser through their respective preburners. Only a small amount is consumed there--just enough to run the turbines; the rest flows through to the combustion chamber.

This "full-flow staged cycle" design has an important advantage: with more mass passing through the turbine that drives the turbopump, the turbopump is driven harder, thus reaching

higher pressures. Higher pressures equal greater performance from the rocket, when top materials are used in manufacturing the shell of the rocket engine.
An image of the recently tested IPD motor is given by NASA in Fig. 1.

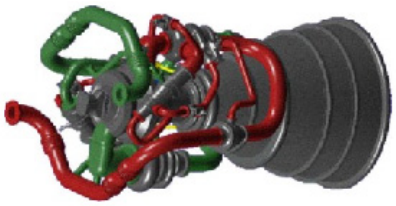

Figure 1. IPD motor 2005.

In estimating the optimal pressure level in the rocket motor a key role resides in the correct computation of the strength of the envelope.

2. Loading capacity of the envelope

A particular method of computation is used to assess the total strains induced in the motor's hood, involving the juxtaposition of the separate pressure and temperature strains [2]. This means the following equations are matched by the axial εx, circumferencial εy and temperature εtemp strains affecting the inner envelope of the motor:

$$\begin{cases} \varepsilon_{x\,tot} = \varepsilon_x + \varepsilon_{temp}, \\ \varepsilon_{y\,tot} = \varepsilon_y + \varepsilon_{temp}, \end{cases} \quad (1)$$

where the "equivalent" stress-strain dependence for the envelope material, at the actual temperature of the wall, must be taken into account,

$$\sigma_i = \sigma_i(\varepsilon_i, t). \quad (2)$$

A rupture theory must be first applied, e.g.

$$\varepsilon_i = \frac{2}{\sqrt{3}}\sqrt{(\varepsilon_x)^2 + \varepsilon_x\varepsilon_y + (\varepsilon_y)^2},$$
$$\sigma_i = \sqrt{(\sigma_x)^2 - \sigma_x\sigma_y + (\sigma_y)^2}. \quad (3)$$

The axial Nx and circumferencial Ny specific loads are respectively given by

$$N_x = \int_{-h/2}^{h/2} \sigma_x(z)\,dz,$$
$$N_y = \int_{-h/2}^{h/2} \sigma_y(z)\,dz. \quad (4)$$

The local shape of the envelope forces a supplemental relation between the two loads be complied with

$$K = \frac{N_x}{N_y}, \quad (5)$$

where the ratio K is, for the particular case of the cylindrical thrust chamber,

$$K = \frac{p_c\pi R^2 - F}{2p_c\pi R^2}. \quad (6)$$

The following formula thus relies the total strains and the chamber pressure

$$\varepsilon_{x\,tot} = \frac{1-2K}{K-2}\varepsilon_{y\,tot} + A, \quad (7)$$

where

$$A = 3\frac{1-K}{2-K}\frac{\int_{-h/2}^{h/2}\frac{\sigma_i}{\varepsilon_i}\varepsilon_{temp}\,dz}{\int_{-h/2}^{h/2}\frac{\sigma_i}{\varepsilon_i}\,dz}. \quad (8)$$

These relations are valid for the self-supported inner envelope of the MRE-1B motor and are easily expandable to the case when a double wall construction is used.
The following loading diagrams for the chamber and nozzle throat regions resulted with the specific parameters of MRE-1B engine (Figure 2).

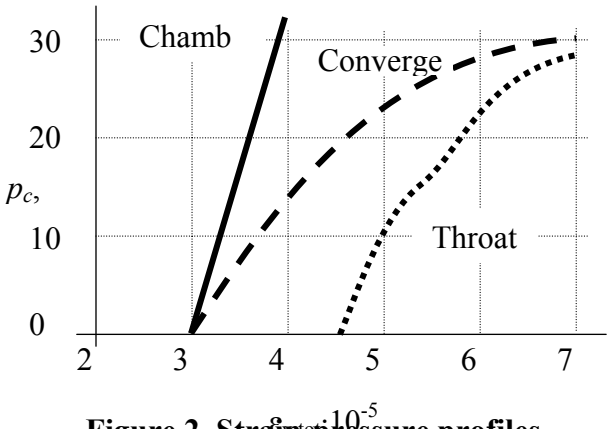

Figure 2. Strain-pressure profiles.

The chamber proves a very high loading capacity, while the most loaded zone of the nozzle throat still has a strain reserve of 14.3 times the inner nominal pressure.
Once the method tested a CAD management of the optimisation is easily implemented. The scope of the entire research is to find the best solutions for the NERVA rocket engine and vehicle.

3. The NERVA Rocket Engine

The basic design is a considerable enhancement of the previous MRE-1B and MRL-26 liquid motors, developed by ADDA and UPB during the past decades. The propellant solution adopted is of a storable double propellant, involving nitrogen tetroxide or nitric acid as oxidiser. In the MRE-1 program a low-pressure, voluminal gear-pump, diergolic main propellant feed system was selected to accomplish the safety requirements.

The following main issues were targeted as research objectives of the preliminary program:

a) The study of injector head efficiency and related thrust chamber optimal shape, length and volume;

b) Study of ignition delays and transients in a triple-component, hypergolic start fuel system;

c) Extensive testing of nitric acid and nitrogen tetroxide based propellants;

d) Thermal transfer in the real cooling system

e) Behaviour of the overall rocket engine system and its controllability;

f) Overall efficiency of the **LRM** as compared to computed thermochemical simulations;

g) Materials behaviour and technology enhancements;

h) Reliability of the liquid propellant rocket propulsion system, in parts and as a whole;

To acquire the largest possible quantity of data during the experiments, an automated monitoring system was naturally introduced. Again to fairly reduce costs, the following main set of engine's parameters was accordingly chosen to be measured, displayed and recorded on the control panel:

1. Turning rate of pumps shafts for oxidiser and fuel;
2. Main propellant delivery pressure at exit of pumps;
3. Main propellant flow rate of components at engine entrance
4. Feed pressure for the auxiliary starting fuel

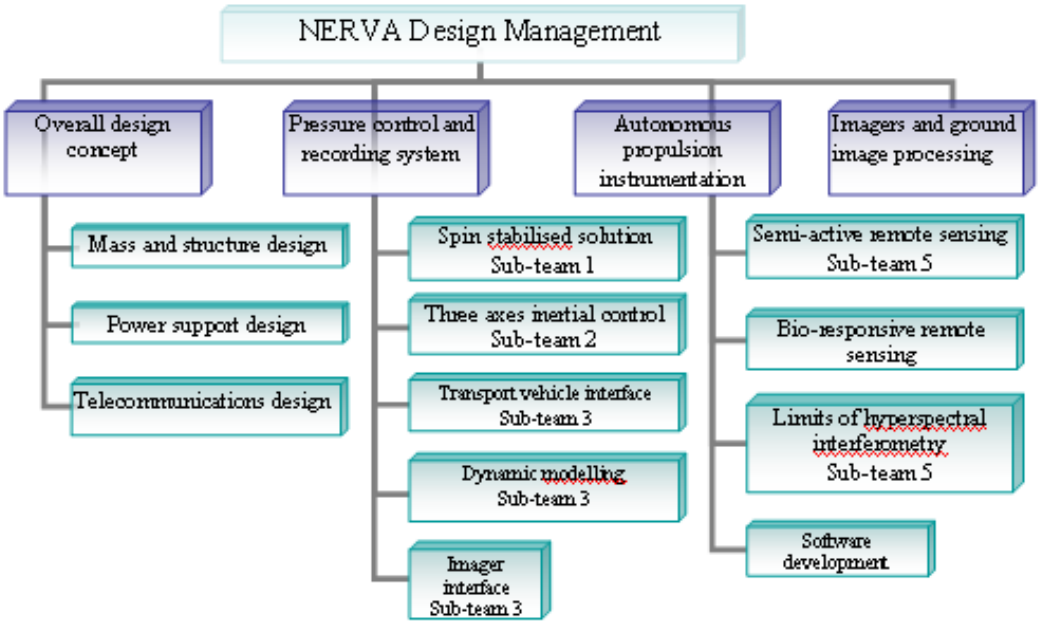

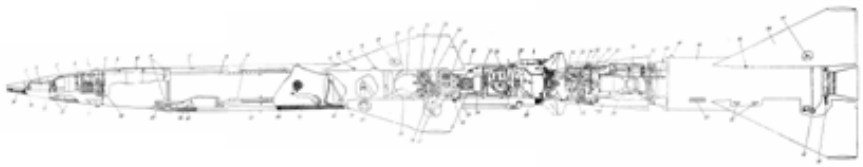

Unsteady axial gas-dynamic thrust;
Pressure level in the thrust chamber;
Ignition delay;
Cooling water temperature.

A voluntarily imposed main constraint for the design is to employ as much as possible existing common equipment in the research. It is the intention to demonstrate in that manner the capability of rocket engine vehicles manufacturing in the environment of the existing Romanian industrial infrastructure. Thus far a minimal number of system devices will be designed and manufactured by the research team.

4. The NERVA Vehicle

Either of small size, the presumed vehicle for eventual satellites launch may be developed starting from an existing propulsion system. Just from the beginning the payload addressed must be substantially evaluated. The case of a formation flight a tethered system will prove highly useful.
Regarding the attitude control system, the two possible solutions are the spinning satellite and the vertically stabilised, thrusters-controlled satellite.

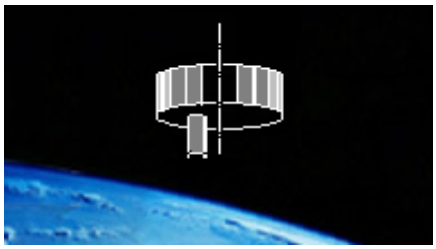

Figure 3. The small observation satellite.

In any of those choices, an optical adaptive system must supplement the attitude controller of the satellite. The objectives considered in the design of the small transporter are sketched below. It is currently studied at UPB based on hundreds of existing soil-to-air missiles of SAM-2 type, stored at present for disposal (draft above). The future minimal launch vehicle makes profit of clustering technology, minimal refurbishing and re-design of the base carrier sections to raise its end velocity.
The transport capacity of some of the variants of the orbital transporter could range between 10 and 50 kg per flight, depending on the value of some unknown parameters related to the envisaged technology. The promoted alternative yet is a three stage configuration of solid-liquid-liquid type. Although a very small system, where usually the specific costs are high, it is expected for the actual costs to remain well below 1000 $/kg LEO payload.
Some of the applications envisaged are also important in defining the features of the future launcher.

5. Re-entry Base Pressure Research

Confident values for base pressure on hypersonic cylindrical bodies were searched from a number of sources. Early works like [1] emphasised on the complex flow behind blunt bodies. Careful and detailed presentations of experimental data are found in the papers by Wilson and Millard [2] for rocket vehicles, and that by Ledu and Pollak, where a re-entry nose cone was tested at Mach 15 on vertical descent trajectories [3]. Impressive base pressure (BP) measured data were shown.
Our reduction and comparison of these data had revealed however that, besides some usual differences, common to all experiments, marked, quite unexpected discrepancies at velocities higher than Mach 4 appear. The resulting analysis shows a need for a deeper insight in the physics of the phenomena, where the main player is the boundary layer. The development of a boundary layer at hyper velocities is further seen to be responsible.
Flight data from flown *Sandhawk* family of rocket vehicles are presented in [2], with base drag estimates by merged processing of radar tracking data on one-hand and static firings of the engine on the other. In [3] a re-entry body with the profile given in the draft below (Fig. 4) was subjected to forced, high altitude fall and BP measurements.

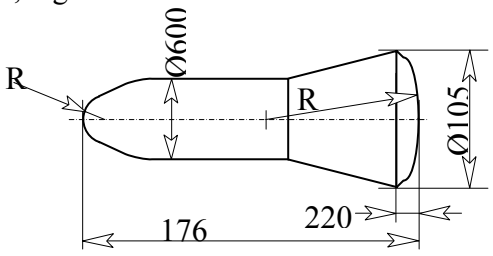

Figure 4. The investigated geometry.

While the velocity interval covered lays between Mach 1 and Mach 15, the base pressure deduction for the Earth atmosphere entry was limited to Mach 7, as published in the reference

paper [3, Fig.6]. Measurements of aerodynamic forces up to Mach 7 are available in [2].

6. Base Pressure Data Reduction

Up to about Mach 4, the reduced BP data fit conveniently with usual flow models, but the problem arises at higher speeds.

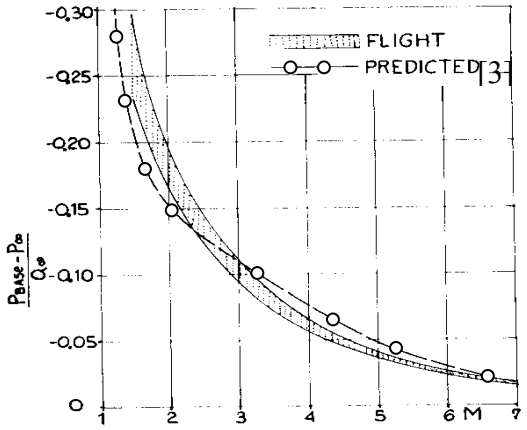

Figure 5. Base perturbation versus Mach number [3].

The pressure perturbation method used for original diagrams means

$$r(M_\infty) = \frac{(p_b - p_\infty)(M_\infty)}{Q_\infty(M_\infty)}. \qquad (11)$$

where the dynamic pressure Q_∞ of the free stream at given Mach number is given by

$$Q_\infty(M_\infty) = \frac{\gamma}{2} p_\infty M_\infty^2, \qquad (12)$$

with p_b the absolute pressure at the corner of the base of the re-entry body [3] and $\Delta p(M_\infty) = p(M_\infty) - p_\infty$ the actual perturbation.

The reduction to the absolute pressure ratio means to change to

$$\frac{p_b}{p_\infty} = 1 - \frac{\gamma}{2} M_\infty^2 r(M_\infty), \qquad (13)$$

where p_∞ is the static air pressure at the altitude of flight. The original plot of $r(M_\infty)$ is given in Fig.2, with our prediction added. Predictions show a decreasing tendency at high velocities then the in-flight data show.

The experiments (grey band) suggest that the trailing vacuum tends to stabilise at a non-zero perturbation level. If this should be the case the variation of the absolute base pressure were the one in Fig. 6, where the resulting p_b / p_∞ is plotted.

In these terms however, a visible increasing of the pressure in the near trailing wake, at Mach 3 and after, is rendered by the French tests. The other predictions give a slowly decreasing pressure level there, as the measurements of Wilson & Millard [2] similarly show.

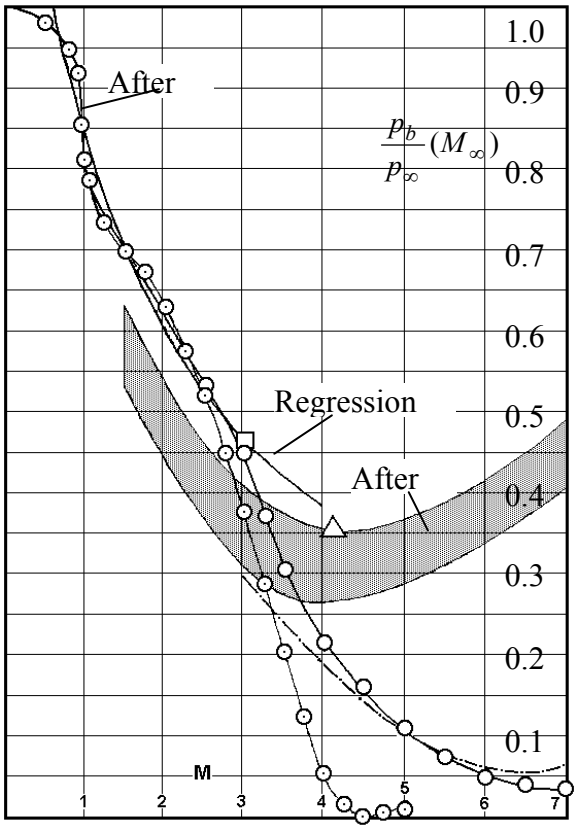

Figure 6. Absolute BP versus Mach number.

Increased absolute pressure in the strong wake after the body does only appear in the measurements [3], where it is clearly shown that after Mach 4 the entire doted zone manifests a considerable raise of more then 40%, after the minimum value of 0.3 in the pressure ratio occurs. The corresponding reduction of the data after [2] (circles in Fig.6), where the drag coefficient was presented, shows an unexplainable decrease around Mach 4, followed by a faint increase and a drop to non-physical negative values.

The aspect of the BP values derived from the rocket vehicle, base drag measurements should

be in fact identical, as far as the definition of the base drag coefficient is the same,

$$c_b(M_\infty) = \frac{p_\infty - p_b}{\frac{\gamma}{2} M_\infty^2 p_\infty} = \frac{p_\infty - p_b}{Q_\infty} = -r(M_\infty) \,. \quad (14)$$

A possible explanation stands in the fact that data as for the pressure perturbation seems being less reliable in graphical representations.
Here slant approximations could generate non-realistic values, while physical explanations of a wake pressure increase can't be excluded.

7. Near Wake Flow

The flow behaviour behind the entry apparatus is complex in fact and possible explanation of velocity dependent BP must be searched regarding the hypersonic expansion and the boundary layer [16]. Ordinary hypersonic flow modelling shows that the stream lines must obey to the rule of Pradtl-Meyer when expanding around a sharp corner and a limiting angle of the flow appears,

$$\theta = \frac{1}{\lambda} \arctan\left(\lambda \sqrt{M_\infty^2 - 1}\right) - \arctan\sqrt{M_\infty^2 - 1} \quad (15)$$

where $\lambda = \sqrt{(\gamma - 1)/(\gamma + 1)}$. This theory is not recommended at M>4, where discontinuous phenomena may appear, but provided the equations were still valid, the limiting angle of the flow shows the values in table 1.

Table 1. Limiting angle of the expansion

Mach	θ °	p / p_∞
4	65.78	0.006586
5	76.92	0.001890
6	84.96	0.000633
7	90.97	0.000339

The pressure ratio was derived from

$$\frac{p}{p_\infty} = \left(1 + \frac{\gamma - 1}{2} M^2\right)^{\frac{\gamma}{1-\gamma}} . \quad (16)$$

It is obvious that the expansion only happen when the flow is free of obstacles. The side-flows around the axially symmetrical body are however colliding and produce a system of detached shocks.
The higher pressure from after the compression wave transmits into the upwind flow through the subsonic boundary layer, developed behind the base and in the entire space around the body. Alternative models of turbulence were used in numerical simulation of the type in [15], [17], [18], which still require further development to meet experiments.
The interfering hypersonic flows produce the base effect even earlier due to the curved shape of the after-body in Fig. 4. High amplitude pitch and conning of the tested nose cone (±3°) should also be responsible for the earlier penetration of the down-stream over pressure on the base of the body at M>4.

8. Far entry applications

The problem is applied in predicting the aerodynamic characteristics of vehicles for the Titan dense atmosphere entry as sound information on base pressure values are also important for accurate optimisation of atmospheric ascent from celestial bodies with dense atmosphere like Earth and Titan. This item is related to far future return missions envisaged from Titan, as the work on discontinuous optimal ascent presented by the author at IAC-55 in Vancouver [19]. The configuration of the entry body is designed to accommodate the return vehicle, with its very high L/D aspect ratio.
Stability aspects have the deciding impact on the configuration and aeromechanical design of the Titan entry body, aggravated by the inconvenient aspect ration. The fluctuating behaviour of the wake and the resulting base pressure are highly important.

9. Conclusions

For the validation of data regarding the base pressure measurements on hypervelocity entry bodies the values of the absolute base pressure proved being more reliable then the usual

pressure perturbation as in aerodynamics and are first recommended.

References

[1] 4. V. I. Feodosiev (1963) *Calculus of strength for the thermally loaded parts of liquid propellant rocket engines*, Moscow.

[2] Wilson, G. G., Millard, W. A. (1971) *Performance and Flight Characteristics of the Sandhawk Family of Rocket Systems*, J. Spacecraft, 8, 7.

[3] Ledu, J., Pollak, C. (1969) *Flight Testing Results on a Hypersonic Re-Entry Nose Cone*, J. Spacecraft, 6, 9, p. 1044-1047.

[4] Rugescu, R. D. (2001) *Thrust and Drag of Variable Mass Aerospace Vehicles*, "Nicolae Tipei" Memorial Symposium, Bucharest, Romania, July 12-13, 2000, Scientific Bulletin of U.P.B., series D Mechanical Engineering, 63, 1, pp. 29-38.

[5] Oswatitsch, K. (1959) *Antriebe mit Heizung bei Uberschahlgeschwindigkeit*, DVL-Berichte No. 90.

[6] Miller, Jay. (2001) *The X-Planes: X-1 to X-45. North Branch*, Minn.: Specialty Press.

[7] Noordung, Hermann. The Problem of Space Travel: The Rocket Motor, edited by Stuhlinger, E., Hunley, J.D., Garland, J., NASA SP-4026, Washington, D.C., 1995.

[8] Rothmund, Christophe (1992) *History of the Viking Engine, Elder*, Donald C., ed. History of Rocketry and Astronautics. ,AAS History Series, 22, San Diego, CA, American Astronautical Society.

[9] Rothmund, Chr., Hopman, H., Kirner, E. (199) *The Early Days of LOX/LH2 Engines at SEP & MBB, AAS History Series*, 21, San Diego, CA, AAS, 7.

[10] Jung, Philippe (1997) *History of Rocketry and Astronautics*, AAS History Series, 21, San Diego, CA, AAS.

[11] Von Kármán, Theodore, and Edson, Lee. (1967) *The Wind and Beyond, Boston, Little, Brown*.

[12] Winter, Frank H. (1990) *Rockets into Space*, Cambridge, MA, Harvard Univ. Press.

[13] Huzel, D. K., (Ed.), Huang, D. H. (Ed.), *Modern Engineering for Design of Liquid-Propellant Rocket Engines*, (Progress in Astronautics and Aeronautics, 147).

[14] Sutton, G. P. (1992) *Rocket Propulsion Elements: An Introduction to the Engineering of Rockets*, John Wiley & Sons; 6th edition.

[15] Waskiewicz, J. D., Shang J. S., Hankey W. L. (1980) *Numerical Simulation of Near Wakes Utilizing a Relaxation Turbulence Model*, AIAA J., 18, 12, pp. 1440-1445.

[16] J.E. Hubbart et al. (1981) *Mach-3 Hydrogen Extermal*/Base Burning, A.I.A.A. Journal, 19, 6, 745-749.

[17] Friedrich, R., Hannappel, R. (1993) *On the Interaction of Wave-Like Disturbances with Shocks-Two Idealizations of the Shock*/Turbulence Interaction Problem, Acta Mecanica, supplement issue.

[18] Hannappel, R., Friedrich, R. (1993) *Interaction of Isotropic Turbulence with a Normal Shock Wave*, Applied Scientific Research, 51, p.507-512.

[19] R.D.Rugescu (2004) *Singular Variational Method Savings in Far Return from Titan*, Paper IAC-04-IAF-A.17, 55th IAF Congress, Vancouver, Canada, October 4-8.

[20]. E.Messerschmid, S.Fasoulas (2000) *Raumfahrt-systeme*, Springer Verlag, Berlin, New York.